Microfluid Nanofluid (2011) 10:1233–1245
DOI 10.1007/s10404-010-0754-5

ORIGINAL PAPER

Analytical model of microfluidic transport of non-magnetic particles in ferrofluids under the influence of a permanent magnet

Taotao Zhu · Darcy J. Lichlyter · Mark A. Haidekker · Leidong Mao

Received: 14 October 2010 / Accepted: 30 November 2010 / Published online: 14 January 2011

Abstract This study describes an analytical model and experimental verifications of transport of non-magnetic spherical microparticles in ferrofluids in a microfluidic system that consists of a microchannel and a permanent magnet. The permanent magnet produces a spatially non-uniform magnetic field that gives rise to a magnetic buoyancy force on particles within ferrofluid-filled microchannel. We obtained trajectories of particles in the microchannel by (1) calculating magnetic buoyancy force through the use of an analytical expression of magnetic field distributions and a nonlinear magnetization model of ferrofluids, (2) deriving governing equations of motion for particles through the use of analytical expressions of dominant magnetic buoyancy and hydrodynamic viscous drag forces, (3) solving equations of motion for particles in laminar flow conditions. We studied effects of particle size and flow rate in the microchannel on the trajectories of particles. The analysis indicated that particles were increasingly deflected in the direction that was perpendicular to the flow when size of particles increased, or when flow rate in the microchannel decreased. We also studied "wall effect" on the trajectories of particles in the microchannel when surfaces of particles were in contact with channel wall. Experimentally obtained trajectories of particles were used to confirm the validity of our analytical results. We believe this study forms the theoretical foundation for size-based particle (both synthetic and biological) separation in ferrofluids in a microfluidic device. The simplicity and versatility of our analytical model make it useful for quick optimizations of future separation devices as the model takes into account important design parameters including particle size, property of ferrofluids, magnetic field distribution, dimension of microchannel, and fluid flow rate.

Keywords Microfluidics · Separation · Particle transport · Ferrofluid · Magnetic buoyancy force

T. Zhu
Department of Chemistry, Nanoscale Science and Engineering Center, The University of Georgia, Athens, GA 30602, USA

D. J. Lichlyter · M. A. Haidekker · L. Mao (✉)
Faculty of Engineering, Nanoscale Science and Engineering Center, The University of Georgia, Athens, GA 30602, USA
e-mail: mao@uga.edu

1 Introduction

Recently, microfluidic particle separation has drawn a lot of attentions, mainly because of its potential diagnostic and therapeutic applications such as in cancer diagnosis (Li et al. 2002; Nagrath et al. 2007), blood cleansing (Toner and Irimia 2005; Yung et al. 2009), pathogen detection (Easley et al. 2006; Cho et al. 2007), and so on. A range of techniques have been developed to manipulate particles based on their intrinsic physical properties (e.g., size, shape, density, compressibility, polarizability) in microfluidic devices, as detailed in three excellent reviews by Pamme (2007), Tsutsui and Ho (2009), and Gossett et al. (2010). These label-free microfluidic techniques are sometimes preferred over conventional ones such as fluorescence-activated cell sorter (FACS) (Bonner et al. 1972) and magnetic-activated cell sorter (MACS) (Miltenyi et al. 1990) because microfluidic techniques are cost-effective, require little user training for operation, and do not rely on the fluorescent or magnetic labels (Kumar and Bhardwaj 2008; Gossett et al. 2010). Among label-free techniques, those based on channel design (e.g., pinched flow fractionation (Yamada et al. 2004) and hydrodynamic filtration

(Yamada and Seki 2005)) and deterministic lateral displacement (Huang et al. 2004; Davis et al. 2006) combine laminar flows with microchannel geometries or micropost array to direct particles of different sizes into separate flow streamlines. Deterministic hydrodynamics separation is capable of separating sub-micron particles as well as DNA molecules with 10 nm resolutions (Huang et al. 2004; Davis et al. 2006). Continuous inertial separation of particles, recently reviewed by Di Carlo (2009), uses balance between inertial lift force and Dean drag forces in curved microchannel for size-dependent separation of particles and cells. In addition to these schemes, researchers are also interested in particle sorting using external energy inputs. For example, techniques based on acoustophoresis can separate particles and cells according to their size, density, as well as compressibility at very high throughput (Laurell et al. 2007; Petersson et al. 2007; Shi et al. 2009). Dielectrophoretic force (DEP), arising from interactions of a cell's induced dipole and its surrounding spatial gradient of electrical field (Voldman 2006), has potential to realize low-cost and integrated devices for high-throughput manipulation of cells. Magnetophoresis uses functionalized magnetic beads to label and separate target particles and cells (Pamme and Manz 2004; Pamme 2006; Pamme and Wilhelm 2006) except in the cases of manipulation of red blood cells and magnetotactic bacteria, both of which are paramagnetic by themselves (Schuler and Frankel 1999; Zborowski et al. 2003; Han and Frazier 2004; Lee et al. 2004). Applications of magnetophoresis in microfluidics have been detailed by three excellent reviews by Pamme (2006), Liu et al. (2009), and Gijs et al. (2010).

More recently, a new approach to magnetically manipulate and sort particles and cells has been developed using ferrofluids (Yellen et al. 2005; Kose et al. 2009; Krebs et al. 2009; Zhu et al. 2010). Ferrofluids are colloidal suspensions of magnetic nanoparticles (Rosensweig 1985). The nanoparticles, usually magnetite (Fe_3O_4) with approximately 10 nm diameter, are covered by surfactants to keep them apart, and suspended within a compatible liquid medium. The liquid medium is typically water for biomedical applications. Ferrofluid hydrodynamics (ferrohydrodynamics), which deals with mechanics of ferrofluid motion under external magnetic fields, has been studied extensively in the past 50 years (Rosensweig 1985). The majority of scientific findings, as well as the applications of ferrofluids, has been summarized in several books by Rosensweig (1985), Berkovsky et al. (1993), and Odenbach (2002). In applications of particle manipulation, the purpose of using ferrofluids is to induce an effective magnetic dipole moment within the non-magnetic object immersed in ferrofluids. The object will experience a magnetic buoyancy force under non-uniform magnetic fields (Rosensweig 1966). This phenomenon has been used to order synthetic particles to form two-dimensional crystalline structures within ferrofluids (Skjeltorp 1983; Pieranski et al. 1996). Ferrofluids in the past have also been used for separating ores by their densities (Rosensweig 1985; Rosensweig et al. 1987). In this case, non-uniform magnetic fields were used to create magnetic pressure distribution in the ferrofluid, which acted as if it had variable density at different height. The similar principle was recently applied by Whitesides' group to separate large synthetic particles according to their densities' difference in paramagnetic salt (e.g., $MnCl_2$, $GdCl_3$) solutions (Winkleman et al. 2007; Mirica et al. 2009, 2010). Pamme's group also demonstrated continuous particle focusing and separation using paramagnetic salt solution in microfluidic devices (Peyman et al. 2009). Magnetic susceptibility of a typical paramagnetic salt solution is about 5–6 orders of magnitude weaker than that of a typical ferrofluid. For example, 1 M concentration of $MnCl_2$ has a susceptibility of $\sim 10^{-6}$, while a ferrofluid with 10% volume ratio has a susceptibility of ~ 1 (Rosensweig 1985; Mirica et al. 2009). Weaker susceptibility of paramagnetic salt solution typically translates to slower manipulation and separation speed. Lately, Friedman's group demonstrated transportation and assembly of colloidal particles inside ferrofluids on top of a substrate with microfabricated periodic micromagnets and suggested a particle sorting scheme (Yellen et al. 2005). Yellen's group successfully created linearly ordered cellular structures inside a bovine serum albumin (BSA) passivated magnetite ferrofluid with a simple electromagnet (Krebs et al. 2009). Koser's group studied the traveling wave magnetic field effect on the ferrofluids dynamics at both macro- and micro-scale (Mao and Koser 2005, 2006). They found a strong dependence of ferrofluid pumping magnitude on both the magnetic field excitation frequency and the traveling magnetic field wavelength. The traveling wave magnetic field was later used to demonstrate an integrated microfluidic platform for controlled sorting of micron-sized particles and live cells within a citrate stabilized cobalt-ferrite ferrofluid in static flow conditions (Kose et al. 2009). Mao's group demonstrated a high-efficiency and high-throughput continuous flow particle separation scheme in ferrofluids in a microfluidic device incorporating a simple hand-held permanent magnet (Zhu et al. 2010). Permanent magnet-based devices have a number of advantages over the ones with microfabricated micromagnets or current-carrying electrodes in that they do not need expensive microfabrication process and auxiliary power supply. They are easy to operate and do not generate heat. The magnetic field produced by permanent magnet is substantially larger than the ones produced by the micromagnets and electrodes. As such, permanent magnet-based devices hold great

potentials for low-cost and user-friendly particle and cell separation systems with high-efficiency and -throughput.

However, using water-based ferrofluids with high concentration of magnetic nanoparticles for live cell manipulation and separation has been proven to be difficult in the past (Kose et al. 2009). The material of nanoparticles, pH value, and stabilizing surfactant of the ferrofluid need to be rendered bio-compatible with live cells, while the overall colloidal system of ferrofluids must be maintained. Typically, nanoparticles within the ferrofluid for biological applications are made of magnetite (iron oxide) (Odenbach 2002; Pankhurst et al. 2003). The advantage of magnetite is that it is air stable against further oxidation and is biocompatible even if the outer surfactant layers covering the nanoparticles disassociate (Weissleder et al. 1989; Muldoon et al. 2005). Magnetite particles have also been approved for uses as magnetic resonance imaging (MRI) contrast agents by Food and Drug Administration (FDA) in the United States (Willard et al. 2004). The pH value of ferrofluids needs to be compatible with the cell culture and maintained at 7.4. Stabilizing surfactant for ferrofluid preparation must be carefully chosen to reduce the possibility of cell death. Two groups successfully demonstrated the synthesis of bio-compatible ferrofluids for live cell manipulation. Yellen's group used BSA to passivate magnetite nanoparticles (Krebs et al. 2009), while Koser's group used citrate to stabilize cobalt-ferrite nanoparticles (Kose et al. 2009). Viability tests from both groups have shown that live cells were able to retain their viability for up to several hours within the ferrofluids. Another issue associated with using ferrofluids for particle and cell manipulation and separation is their opaqueness. Reason for the opaqueness of ferrofluids can be explained from considerations of magnitude of optical depth $\tau = n\sigma l$ (Rosensweig 1966), where n is concentration of magnetic nanoparticles in the ferrofluid, σ is optical cross-sectional area of a nanoparticle, i.e., geometric projected area of the nanoparticle, and l is length of optical path. If we define I_0 as fluorescent intensity of particle, and I as observed intensity after a given optical path through ferrofluids, $I/I_0 = e^{-\tau}$. It is clear that ferrofluids with relatively low solid volume fraction are preferred for particle observation because of their small optical depth. In reality, particles or cells within ferrofluids need to be both fluorescently labeled and close to the channel surface for direct observation under microscope.

In this paper, we developed an analytical model to describe transport of non-magnetic particles within ferrofluids in a microfluidic system consisting of a microchannel and a permanent magnet. Numerical models using finite element analysis (FEA) have been developed in the past for magnetophoretic particle transport within microfluidic devices, in which the particles themselves were magnetic, while the surrounding medium was non-magnetic (Pham et al. 2000; Smistrup et al. 2005; Gassner et al. 2009). The accuracy of numerical approaches depends heavily on mesh quality. They are not suitable for parametric studies aimed for quick device design and optimization. Analytical models were developed to enable accurate and fast parametric analysis of large-scale magnetophoretic systems (Furlani 2006; Furlani and Sahoo 2006). However, few have considered the opposite case, where the particles were non-magnetic and the surrounding medium was magnetic (e.g. ferrofluids). We derived the equations of motion for particles in ferrofluids using analytical expressions for dominant magnetic and hydrodynamic forces. The magnetic force is obtained by using an analytical expression of magnetic field distributions in microchannel, in conjunction with a non-linear magnetization model of ferrofluids. The model developed here can predict the transport of non-magnetic particles in ferrofluids under the influence of a permanent magnet in a microchannel. The model is also able to perform parametric analysis for quick device optimizations.

2 Theory

2.1 Force analysis

The system considered in the model consists of a microfluidic channel and a permanent magnet, as illustrated in Fig. 1a. Dimensions of the channel and the magnet are labeled in Fig. 1b, c. The microfluidic channel is filled with ferrofluids. Non-magnetic spherical particles are introduced into the microchannel via inlet at the center point. Without external magnetic fields, the particles are expected to exit the channel outlet at the center point, too. When a rectangular permanent magnet is placed at the center of channel length with its direction of magnetization perpendicular to channel wall, the bias field magnetizes the ferrofluid within the microchannel and subsequently deflects the particles' trajectories. The trajectories can be analyzed by considering dominant magnetic and hydrodynamic forces in the equations of motion. Typically, particle transport in ferrofluids under external magnetic fields is governed by various forces and interactions including magnetic buoyancy force, hydrodynamic viscous drag force, gravity, buoyancy force, particle and microchannel surface interaction (van der Waal's force, electrostatic force and lubrication force), diffusion due to Brownian motion, particle and fluid interaction, interparticle effects (magnetic dipole–dipole interaction). For micron-sized particles in ferrofluids, only the magnetic and viscous forces are dominant. For example, we compute the gravitational and buoyant forces, $F_g = \frac{4}{3}\rho_p \pi R_p^3 g$, and $F_b = \frac{4}{3}\rho_f \pi R_p^3 g$. For a 2 μm ($R_p = 1$ μm) polystyrene particle in

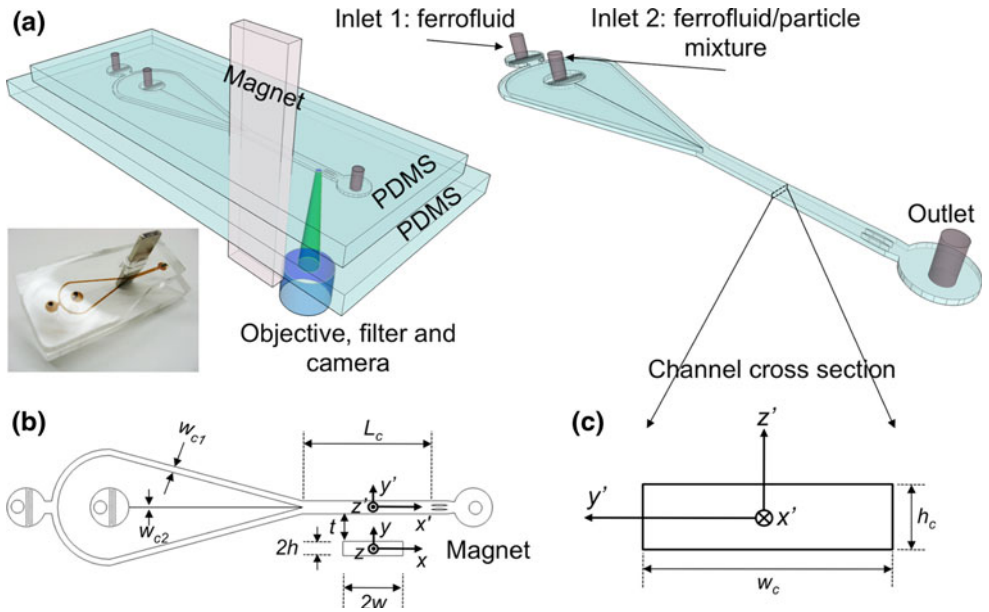

Fig. 1 **a** Schematic representation of the microfluidic system with a permanent magnet and a microchannel. Non-magnetic microparticles and ferrofluid mixture were introduced into the microfluidic channel Inlet 2 and hydrodynamically focused by the ferrofluid sheath flow from Inlet 1. Upon entering the main channel, deflection of microparticles from their flow paths occurred because of non-uniform magnetic fields produced by a long NdFeB permanent magnet embedded into the microfluidic channel. The motion of the particles was imaged through a ×5 objective and a CCD camera. *Inset* shows an image of the fabricated device. **b** The dimensions of the microfluidic channel and the magnets, and their relative locations. $L_c = 1$ cm, $2w = 6.35$ mm, $2h = 1.59$ mm, $t = 2.24$ mm, $w_{c1} = 485$ μm, $w_{c2} = 30$ μm. x–y coordinate system is within the permanent magnet, with its origin at the center of the cross-section of the magnet. x'–y' coordinate system is within the microchannel, with its y' origin at the half width of the microchannel. **c** The cross-section of the microfluidic channel. $h_c = 26$ μm and $w_c = 1{,}000$ μm

EMG 408 ferrofluid ($\rho_p = 1050$ kg/m^3, $\rho_f = 1070$ kg/m^3, $g = 9.8$ m/s), we obtain $F_g = 4.31 \times 10^{-2}$ pN, and $F_b = 4.39 \times 10^{-2}$ pN, both of which are approximately two orders of magnitude smaller than magnetic buoyancy force (∼pN). The molecular and electrical interaction between particles and surfaces of microchannel is referred as *Derjaguin–Landau–Verwey–Overbeek* (DLVO) force. DLVO force is a combination of the van der Waal's force and the electrostatic force. Electrostatic force can be either repulsive or attractive, while the van der Waal's force is always attractive. It is usually beneficial to treat surfaces of microchannel chemically and render the electrostatic force repulsive to avoid problems of particles sticking to channel surfaces (Liu et al. 2009). DLVO force can be neglected after the proper surface treatment. The close proximity between particles and channel surface also affects the magnitude of hydrodynamic viscous drag force by introducing a non-dimensional factor accounting for the "wall effect" (Ganatos et al. 1980; Krishnan and Leighton 1995; Wirix-Speetjens et al. 2005), which will be discussed in details in Sect. 2.3. Moreover, hydrodynamic lift force (Leighton and Acrivos 1985; Krishnan and Leighton 1995), caused by viscous flow over a particle near channel surface, tries to levitate the particle and produces a lifting force, $F_l = 9.22\ \rho_p R_p^4 \gamma^2$, where γ is shear rate at the channel surface. Magnitude of the lifting force is much smaller than pN and is therefore neglected in the following analysis. When non-magnetic particles are sufficiently small, Brownian motion and diffusion start to affect the trajectories of the particles in ferrofluids. To estimate this effect, we obtain the diffusion coefficient, D, of a particle inside ferrofluids according to the Stokes–Einstein relation (Einstein 1956), $D = \frac{k_B T}{6\pi\eta R_p}$. For a 10 μm ($R_p = 5$ μm) polystyrene particle in a commercially available EMG 408 water-based ferrofluid ($\eta = 1.2 \times 10^{-3}$ kg/m s), its diffusion coefficient is 3.6×10^{-14} m^2/s at room temperature. After 20 s of diffusion, the particle will move an average distance of 0.9 μm. For a 1 μm ($R_p = 0.5$ μm) polystyrene particle, its diffusion coefficient is about one order larger than that of 10 μm particle, and the average diffusion distance increases to 2.7 μm. Even for 1 μm particles, diffusion effect is second order compared to magnetic and hydrodynamic forces. Concentration of non-magnetic particles in ferrofluids is assumed to be low such that interparticle effects and particle/fluid interactions can also be neglected.

2.2 Magnetic buoyancy force

Commercial ferrofluids typically consist of magnetite (Fe_3O_4) nanoparticles with approximately 10 nm diameter. For example, the mean diameter of nanoparticles of EMG

408 ferrofluids from Ferrotec Co. has been determined from transmission electron microscopy (TEM) images to be 10.2 nm with a standard deviation of 1.25 nm (see Fig. 2a). This dilute ferrofluids exhibit superparamagnetic behavior illustrated by the magnetization curve shown in Fig. 2b. The saturation magnetization of ferrofluids is generally low compared to that of ferromagnetic materials. The saturation magnetization of a ferrofluid, M_{SAT}, equals to ϕM_d, where ϕ is the volume fraction of the magnetic content and M_d is the saturation moment of the bulk material. EMG 408 ferrofluid with a solid volume fraction of 1.1% has a saturation magnetization of 5,252 A/m, given that the saturation moment of Fe_3O_4 is 44,600 A/m (Rosensweig 1985). The magnetization curve of a low-concentration ferrofluid can be modeled accurately by considering the magnetic nanoparticles as a collection of individual and non-interacting magnetic dipoles. This approach leads to the Langevin function of ferrofluid magnetization (Rosensweig 1985),

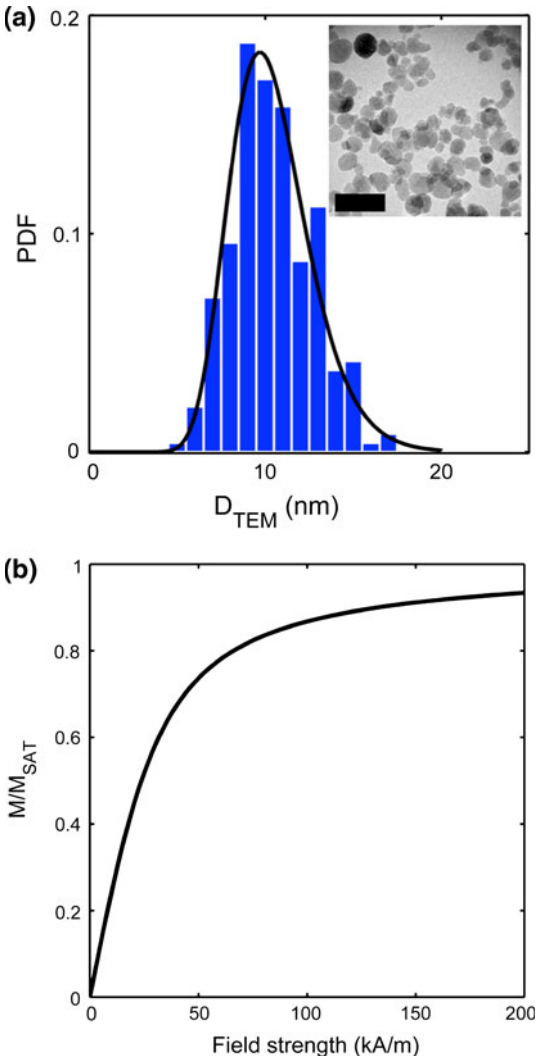

Fig. 2 **a** Probability density function (PDF) for magnetic nanoparticle sizes was obtained via TEM images from 240 individual, randomly selected nanoparticles. Diameter (D_{TEM}) of nanoparticles displays a log-normal distribution (mean, $\mu = 10.2$ nm; standard deviation, $\sigma = 1.25$ nm). *Inset* depicts a typical TEM image of nanoparticles. The scale bar represents 40 nm. **b** The theoretical and normalized Langevin curve as a function of the magnetic field strength. **M** is the magnetization of the ferrofluid and M_{SAT} is the saturation magnetization. The ferrofluid parameters used to construct this curve matches the properties of EMG 408 water-based ferrofluid used in the experiments. EMG 408 ferrofluid is assumed to be superparamagnetic because of its low solid volume fraction

$$\frac{M}{\phi M_d} = \frac{M}{M_{SAT}} = L(\alpha) = \coth(\alpha) - \frac{1}{\alpha} \tag{1}$$

where $\alpha = \frac{\pi \mu_0 M_d H d^2}{6 k_B T}$, μ_0 is permeability of free space, H is magnitude of non-uniform magnetic fields, d is mean diameter of nanoparticle, k_B is Boltzmann constant, T is temperature.

Under non-uniform magnetic fields, particles inside ferrofluids experience a magnetic buoyancy force, $\mathbf{F}_m$. The magnitude of force can be calculated from a Maxwell stress tensor (Rosensweig 1985),

$$\mathbf{F}_m = -\oint_S \left(\frac{1}{2}\mu_0 M_n^2 + \mu_0 \int_0^H M dH \right) \hat{\mathbf{n}} dS \tag{2}$$

where S is surface that just encloses the non-magnetic particle, H is magnitude of non-uniform magnetic fields, $\hat{\mathbf{n}}$ is outward-directed unit normal vector at the particle surface, and M_n is normal component of ferrofluid magnetization adjacent to the surface S enclosing the particle. In the limit of dilute ferrofluid or intense applied magnetic field, $\frac{1}{2}M_n^2/\bar{M}H \ll 1$, where $\bar{M}$ is mean ferrofluid magnetization. Therefore, magnetic buoyancy force on a non-magnetic particle inside ferrofluids can be simply expressed as,

$$\mathbf{F}_m = -V\mu_0(\mathbf{M} \cdot \nabla)\mathbf{H} \tag{3}$$

where V is volume of the non-magnetic particle, **M** is effective magnetization of the ferrofluid surrounding the particle, and **H** is magnetic field strength at the center of the particle. The presence of the minus sign in front of the term indicates non-magnetic particle immersed in ferrofluids experiences a force in the direction of weaker magnetic field. Effective ferrofluid magnetization, **M**, is related to the magnetization of ferrofluid $\mathbf{M}_f$ through a "demagnetization" factor, which accounts for shape-dependent demagnetization of ferrofluids due to presence of the non-magnetic particle. Equation 3 takes magnetic field, **H**, to be the field at the center of the particle inside ferrofluid sample. Experimentally, permanent magnet produces an external field, $\mathbf{H}_e$, in the place where ferrofluid channel is located. It is necessary to determine the value of field inside ferrofluids sample **H** by relating it to applied field $\mathbf{H}_e$.

$$\mathbf{H} = \mathbf{H}_e - c \cdot \mathbf{M}_f \tag{4}$$

where c is "demagnetization" factor of rectangular ferrofluid-filled microchannel. Ferrofluid magnetization $\mathbf{M}_f$ in our case is much smaller than the external field $\mathbf{H}_e$ produced by a Neodymium–Iron–Boron (NdFeB) magnet. As a result, magnetic field at the center of the particle $\mathbf{H}$ can be approximated as external field $\mathbf{H}_e$.

In order to calculate the magnitude of magnetic buoyancy force, we need to know the effective magnetization of ferrofluid, $\mathbf{M}$, adjacent to the particle. The nonlinearity of ferrofluid magnetization makes the identification of the effective magnetization, $\mathbf{M}$, complicated. In a very weak magnetic field ($H \ll H_{SAT}$, where H_{SAT} is magnitude of the minimal magnetic field strength to saturate ferrofluids), we can linearize the Langevin curve to define an initial magnetic susceptibility χ and form an effective dipole moment $-V\chi H$ for the particle. Shape dependent "demagnetization" field needs to be considered under this assumption. In a large magnetic field that saturates ferrofluids, effective magnetic moment of a particle immersed in ferrofluids can be extracted as $-VM_{SAT}$, and particle shape has virtually no influence on this force expression because demagnetization is not significant when $M_{SAT} \ll H$ (Jones 1995). When applied magnetic fields fall in between the above-mentioned extreme cases, we can obtain magnetization of the ferrofluid, $\mathbf{M}_f$, from the Langevin curve and decide whether or not to apply "demagnetization" factor depending on the magnitude of external magnetic fields. In this paper, EMG 408 ferrofluid used in our experiment is dilute, and external magnetic field is much larger than saturation magnetization of this ferrofluid. Therefore, we can assume "demagnetization" field is small enough so that $\mathbf{M}$ equals to $\mathbf{M}_f$. The value of $\mathbf{M}_f$ can be calculated from the Langevin function.

The magnetic buoyancy force can be expressed in both x and y components,

$$\mathbf{F}_m(x,y) = F_{mx}(x,y)\hat{\mathbf{x}} + F_{my}(x,y)\hat{\mathbf{y}} \tag{5}$$

where

$$F_{mx}(x,y) = -V\mu_0\left[M_x\frac{\partial H_x(x,y)}{\partial x} + M_y\frac{\partial H_x(x,y)}{\partial y}\right] \tag{6}$$

$$F_{my}(x,y) = -V\mu_0\left[M_x\frac{\partial H_y(x,y)}{\partial x} + M_y\frac{\partial H_y(x,y)}{\partial y}\right] \tag{7}$$

where

$$M = \phi M_d \times \left[\coth(\alpha) - \frac{1}{\alpha}\right] \tag{8}$$

$$M_x = M \times \cos\left[\tan^{-1}\frac{H_y}{H_x}\right] \tag{9}$$

$$M_y = M \times \sin\left[\tan^{-1}\frac{H_y}{H_x}\right] \tag{10}$$

Analytical solutions for magnetic fields of a single long rectangular permanent magnet of width $2w$ and height $2h$ that is centered with respect to the origin in the x–y plane can be derived as following (Furlani 2006). Assume the magnet has a residual magnetization M_S,

$$H_x(x,y) = \frac{M_S}{4\pi}\left\{\ln\left[\frac{(x+w)^2+(y-h)^2}{(x+w)^2+(y+h)^2}\right] - \ln\left[\frac{(x-w)^2+(y-h)^2}{(x-w)^2+(y+h)^2}\right]\right\} \tag{11}$$

$$H_y(x,y) = \frac{M_S}{2\pi}\left\{\tan^{-1}\left[\frac{2h(x+w)}{(x+w)^2+y^2-h^2}\right] - \tan^{-1}\left[\frac{2h(x-w)}{(x-w)^2+y^2-h^2}\right]\right\} \tag{12}$$

The expressions for the magnetic field gradients are,

$$\frac{\partial H_x(x,y)}{\partial x} = \frac{M_S}{2\pi}\left[\frac{x+w}{(x+w)^2+(y-h)^2} - \frac{x+w}{(x+w)^2+(y+h)^2} - \frac{x-w}{(x-w)^2+(y-h)^2} + \frac{x-w}{(x-w)^2+(y+h)^2}\right] \tag{13}$$

$$\frac{\partial H_x(x,y)}{\partial y} = \frac{M_S}{2\pi}\left[\frac{y-h}{(x+w)^2+(y-h)^2} - \frac{y-h}{(x-w)^2+(y-h)^2} - \frac{y+h}{(x+w)^2+(y+h)^2} + \frac{y+h}{(x-w)^2+(y+h)^2}\right] \tag{14}$$

$$\frac{\partial H_y(x,y)}{\partial x} = \frac{M_S}{\pi}\left\{\frac{h\left[y^2-(x+w)^2-h^2\right]}{\left[(x+w)^2+y^2-h^2\right]+4h^2(x+w)^2} - \frac{h\left[y^2-(x-w)^2-h^2\right]}{\left[(x-w)^2+y^2-h^2\right]+4h^2(x-w)^2}\right\} \tag{15}$$

$$\frac{\partial H_y(x,y)}{\partial y} = \frac{2^*M_S}{\pi}\left\{\frac{hy(x-w)}{\left[(x-w)^2+y^2-h^2\right]+4h^2(x-w)^2} - \frac{hy(x+w)}{\left[(x+w)^2+y^2-h^2\right]+4h^2(x+w)^2}\right\} \tag{16}$$

2.3 Hydrodynamic drag force

When a non-magnetic particle is driven by magnetic buoyancy force and moves in ferrofluids, the resistance

from ferrofluids is named hydrodynamic drag force. The force is caused by the viscosity of medium and can be calculated for a spherical particle in a low Reynolds number flow (Deen 1998),

$$\mathbf{F}_{\mathrm{d}} = 3\pi\eta D_{\mathrm{p}}\left(\mathbf{v}_{\mathrm{f}} - \mathbf{v}_{\mathrm{p}}\right) f_D \tag{17}$$

where η is viscosity of ferrofluids, D_{p} is diameter of spherical particle, and $\mathbf{v}_{\mathrm{f}}$ and $\mathbf{v}_{\mathrm{p}}$ are velocity vectors of ferrofluids and the particle, respectively. f_D is hydrodynamic drag force coefficient of the particle and incorporates the influence of a solid surface in the vicinity of the moving particle ("wall effect"). It is a resistance function of the hydrodynamic interaction between the particle and surface. Its appearance indicates increased fluid viscosity the large particle experiences as it moves close to the microfluidic channel surface (Ganatos et al. 1980; Wirix-Speetjens et al. 2005),

$$f_D = \left[1 - \frac{9}{16}\left(\frac{D_{\mathrm{p}}}{D_{\mathrm{p}} + 2z_{\mathrm{p}}}\right) + \frac{1}{8}\left(\frac{D_{\mathrm{p}}}{D_{\mathrm{p}} + 2z_{\mathrm{p}}}\right)^3 - \frac{45}{256}\left(\frac{D_{\mathrm{p}}}{D_{\mathrm{p}} + 2z_{\mathrm{p}}}\right)^4 - \frac{1}{16}\left(\frac{D_{\mathrm{p}}}{D_{\mathrm{p}} + 2z_{\mathrm{p}}}\right)^5\right]^{-1} \tag{18}$$

where z_{p} is distance between surface of the particle and channel wall.

To evaluate the drag force, we need an expression for the fluid velocity, $\mathbf{v}_{\mathrm{f}}$, in the rectangular microfluidic channel depicted in Fig. 1. Let L_{c} denote length of the channel and h_{c} and w_{c} denote height and width of its rectangular cross-section. The laminar nature of flow is estimated from the Reynolds number $Re = \frac{\rho U_0 L_0}{\eta}$, where U_0 is characteristic velocity of the flow, L_0 is characteristic dimension of the microchannel, ρ and η are density and viscosity of the fluid, respectively. Typically, $U_0 = 0.001$ m/s, $L_0 = 20$ μm, $\rho = 1000$ kg/m^3, $\eta = 0.001$ kg/m s. Therefore, $Re = 0.02$, indicating laminar flow. We assume fully developed laminar flow with the flow velocity parallel to the x'-axis, and varying across its cross-section,

$$\mathbf{v}_{\mathrm{f}} = v_{\mathrm{f}}(y', z')\hat{\mathbf{x}} \tag{19}$$

We choose to use coordinates y' and z' centered with respect to the cross-section of the channel, and this coordinate system differs from the coordinate system used for magnetic field analysis (Furlani and Sahoo 2006). The velocity profile for fully developed laminar flow is expressed as (Brody et al. 1996; Ichikawa et al. 2004),

$$v_{\mathrm{f}} = \left(\frac{\Delta P}{L_{\mathrm{c}}}\right)\left(\frac{4h_{\mathrm{c}}^2}{\eta\pi^3}\right)\sum_{n=0}^{\infty}\frac{(-1)^n}{(2n+1)^3} \times \left\{1 - \frac{\cosh\frac{(2n+1)\pi y'}{h_{\mathrm{c}}}}{\cosh\frac{(2n+1)\pi w_{\mathrm{c}}}{2h_{\mathrm{c}}}}\right\} \times \cos\frac{(2n+1)\pi z'}{2h_{\mathrm{c}}} \tag{20}$$

where ΔP is change in pressure across the length L_{c} of the channel. Channel aspect ratio is defined as $\varepsilon = h_{\mathrm{c}}/w_{\mathrm{c}}$. Under the condition of $0 < \varepsilon < 2$, calculation error is found to be less than 1% when only $n = 0$ and 1 terms are used to represent the flow profile in microchannels (Ichikawa et al. 2004).

$$v_{\mathrm{f}} = \left(\frac{\Delta P}{L_{\mathrm{c}}}\right)\left(\frac{4h_{\mathrm{c}}^2}{\eta\pi^3}\right)\left\{\left[1 - \frac{\cosh\frac{\pi y'}{h_{\mathrm{c}}}}{\cosh\frac{\pi w_{\mathrm{c}}}{2h_{\mathrm{c}}}}\right] \times \cos\frac{\pi z'}{h_{\mathrm{c}}} - \frac{1}{27}\left[1 - \frac{\cosh\frac{3\pi y'}{h_{\mathrm{c}}}}{\cosh\frac{3\pi w_{\mathrm{c}}}{2h_{\mathrm{c}}}}\right] \times \cos\frac{3\pi z'}{h_{\mathrm{c}}}\right\} \tag{21}$$

In a typical microfluidic experiment setup, volumetric flow rate, Q, instead of pressure drop across the channel, is available to the experimenter. Therefore, we rewrite the pressure drop in terms of the flow rate,

$$\Delta P = \frac{QL_{\mathrm{c}}\eta\pi^4}{8w_{\mathrm{c}}h_{\mathrm{c}}^3} \times \left\{\left[1 - \frac{2h_{\mathrm{c}}}{\pi w_{\mathrm{c}}}\tanh\left(\frac{\pi w_{\mathrm{c}}}{2h_{\mathrm{c}}}\right)\right] + \frac{1}{81}\left[1 - \frac{2h_{\mathrm{c}}}{3\pi w_{\mathrm{c}}}\tanh\left(\frac{3\pi w_{\mathrm{c}}}{2h_{\mathrm{c}}}\right)\right]\right\}^{-1} \tag{22}$$

Finally, the expression for fluid velocity, v_{f}, in the rectangular microfluidic channel is,

$$v_{\mathrm{f}} = \frac{Q\pi}{2w_{\mathrm{c}}h_{\mathrm{c}}} \times \left\{\left[1 - \frac{2h_{\mathrm{c}}}{\pi w_{\mathrm{c}}}\tanh\left(\frac{\pi w_{\mathrm{c}}}{2h_{\mathrm{c}}}\right)\right] + \frac{1}{81}\left[1 - \frac{2h_{\mathrm{c}}}{3\pi w_{\mathrm{c}}}\tanh\left(\frac{3\pi w_{\mathrm{c}}}{2h_{\mathrm{c}}}\right)\right]\right\}^{-1} \times \left\{\left[1 - \frac{\cosh\frac{\pi y'}{h_{\mathrm{c}}}}{\cosh\frac{\pi w_{\mathrm{c}}}{2h_{\mathrm{c}}}}\right] \times \cos\frac{\pi z'}{2h_{\mathrm{c}}} - \frac{1}{27}\left[1 - \frac{\cosh\frac{3\pi y'}{h_{\mathrm{c}}}}{\cosh\frac{3\pi w_{\mathrm{c}}}{2h_{\mathrm{c}}}}\right] \times \cos\frac{3\pi z'}{h_{\mathrm{c}}}\right\} \tag{23}$$

2.4 Equations of motion

The equations of motion for a non-magnetic particle in the microchannel are,

$$m\frac{\mathrm{d}v_{p,x}}{\mathrm{d}t} = F_{mx}(x, y) + 3\pi\eta D_{\mathrm{p}}\left(v_{\mathrm{f}} - v_{\mathrm{p},x}\right) f_D \tag{24}$$

$$m\frac{\mathrm{d}v_{p,y}}{\mathrm{d}t} = F_{my}(x, y) - 3\pi\eta D_{\mathrm{p}} v_{\mathrm{p},y} f_D \tag{25}$$

Since the Reynolds number in microfluidic channels is very small, normally on the order of 0.01, viscous effect often dominates over inertial effect. As a result, the left hand side terms of Eqs. 24 and 25 reduce to zero, which leads to,

$$v_{\mathrm{p},x} = \frac{\mathrm{d}x}{\mathrm{d}t} = \frac{F_{mx} + 3\pi\eta D_{\mathrm{p}} v_{\mathrm{f}} f_D}{3\pi\eta D_{\mathrm{p}} f_D} \tag{26}$$

$$v_{p,y} = \frac{dy}{dt} = \frac{F_{my}}{3\pi\eta D_p f_D} \quad (27)$$

With initial conditions $x(0)$ and $y(0)$, these two ordinary differential equations can be solved numerically using Runge–Kutta method. We solved them in MATLAB (Version R2007a, Mathworks Inc., Natick, MA) using ode45 function, which is an automatic step-size Runge–Kutta integration method using a fourth and fifth order pair.

3 Experimental details

A microfluidic device with one NdFeB permanent magnet was fabricated to experimentally study the trajectories of particles, as shown in the inset of Fig. 1a. EMG 408 ferrofluid was used in the experiments. The volume fraction of the magnetite particles for this ferrofluid is 1.1%, corresponding to a saturation magnetization of 5,252 A/m. The viscosity of the ferrofluid was measured to be 1.2 N s/m^2 by a rheometer (DV-III+, Brookfield Engineering Laboratories Inc., Middleboro, MA). Two different sizes (4.8 μm and 7.3 μm in diameters) of green fluorescent polystyrene spherical particles (Thermo Fisher Scientific Inc., Waltham, MA) with a density of 1.05 g/cm^3 were used. The coefficient of variation (the ratio of the standard deviation to the mean) of the particle diameters was less than 5%. Fluorescent particles suspension was first diluted with DI water containing 0.1% Tween 20 to prevent particle aggregation, then mixed with ferrofluids for flow experiments. PDMS microfluidic channel was fabricated through a standard soft-lithography approach and attached to the flat surface of another piece of PDMS (Xia and Whitesides 1998). The mask was created using AutoCAD 2008 (Autodesk Inc., San Rafael, CA) and printed by a commercial photo-plotting company (CAD/Art Services Inc, Bandon, Oregon). Dimensions of the microfluidic channel are listed in Fig. 1. The thickness of the channel was measured to be 26 μm by a profilometer (Dektak 150, Veeco Instruments Inc., Chadds Ford, PA). PDMS surfaces were treated before attachment with plasma (PDC-32G plasma cleaner, Harrick Plasma, Ithaca, NY) at 11.2 Pa O_2 partial pressure with 18 W power for 1 min. The flow experiment was conducted on the stage of an inverted microscope (Zeiss Axio Observer, Carl Zeiss Inc., Germany). Before liquid injection, completed device was exposed again to plasma for 10 min to keep the surfaces hydrophilic. Triton X-100 solution was injected into the channel. The solution was kept in the channel for 20 min then purged with N_2 gas. This step ensured that the polystyrene particles would not attach to PDMS surfaces during experiments. The microfluidic channel was afterwards filled with air-bubble free EMG 408 ferrofluid. During experiments, ferrofluid injection into Inlet 1 was maintained at variable flow rates using a syringe pump (KDS 101, KD Scientific, Holliston, MA). Ferrofluid and particles mixture were injected into Inlet 2 using a second syringe pump (Nexus 3000, Chemyx Inc., Stafford, TX). Non-uniform magnetic field was generated by one NdFeB permanent magnet with the magnetization directed across its thickness. The magnet is 6.35 mm in width, 1.59 mm in thickness and 25.4 mm in length, and was placed 2.24 mm away from microfluidic channel. The magnetic flux density at the center of the magnets' pole surface was measured to be 159.9 mT by a Gauss meter (Model 5080, Sypris, Orlando, FL) and an axial probe with 0.381 mm diameter of circular active area. The images of fluorescent particles were recorded through a fluorescent filter set (41001 FITC, Chroma Technology Corp., Rockingham, VT) and a ×5 objective with a CCD camera (SPOT RT3, Diagnostic Instruments, Inc., Sterling Heights, MI). ImageJ® software was used to record the trajectories and deflections of the particles inside ferrofluids.

4 Results and discussion

We obtained the theoretical trajectories of non-magnetic particles in a microfluidic system depicted in Fig. 1a by solving Eqs. 26 and 27 numerically using ode45 function in MATLAB. Specifically, we studied the spherical particles with variable diameters from 1 to 10 μm in a microfluidic system that consists of a microchannel that is 26 μm high, 1,000 μm wide, and 1 cm long (L_c = 1 cm, h_c = 26 μm and w_c = 1,000 μm). Total flow rate, Q, at the inlet of the microchannel was varied between 5 and 25 μl/min. The ferrofluid in the microchannel had a viscosity of 1.2 N s/m^2 and a saturation magnetization of 5,252 A/m. The volume fraction of the ferrofluid was 1.1%. The mean diameter of nanoparticles was 10 nm. The permanent magnet was placed at the center of the length of the microchannel with its direction of magnetization perpendicular to the flow. The distance between the magnet and the channel was 2.24 mm (edge to edge). Throughout the analysis we assumed that the residual flux density ($\mu_0 M_S$) of the permanent NdFeB magnet was 1.13 T. The magnet was 6.35 mm in width ($2w$), 1.59 mm in height ($2h$) and 25.4 mm in length. These simulation parameters were chosen to match the experimental conditions.

Magnitude of magnetic buoyancy force depends on both the external magnetic fields and the field gradient. It is thus important to model magnetic fields from a permanent magnet with great precision. We chose to use an analytical approach instead of numerical FEA approach to calculate magnetic fields. Analytical solution provides exact values of field and its gradient at each point of interest, while

solutions from FEA depends heavily on the mesh quality, which will likely introduce error into magnetic buoyancy force calculation. Equations 11–16 are analytical solutions of magnetic field and field gradient for an infinitely long permanent magnet with $2w$ width and $2h$ height. The direction of the magnetization is across the magnet's thickness. Analytical solutions, numerical FEA solutions, as well as measurement data from a Gauss meter of magnetic fields were compared for the permanent magnet. FEA solution of the permanent magnet was calculated by magnetostatics solvers in COMSOL Multiphysics (Version 3.5a, COMSOL Inc., Burlington, MA). A 2D solver was used to compute the field in a 0.5 m × 0.2 m region containing the permanent magnet's cross-section (6.35 mm × 1.59 mm) at center. A 3D solver was used to compute the field in a 0.5 m × 0.2 m × 2 m region containing the permanent magnet (6.35 mm × 1.59 mm × 25.4 mm). The magnetic field component perpendicular to the region boundary all went to zero at the boundaries. Figure 3a shows that analytical solutions of magnetic field match both FEA solutions and experimental results reasonably well. Figure 3b depicts the distribution of magnetic fields inside the microfluidic channel using analytical solutions. Figure 3c shows the normalized ferrofluid magnetization inside the microfluidic channel. We concluded that EMG 408 ferrofluid in the microchannel was not fully saturated under the permanent magnet. However, magnetic fields produced by the magnet (40,000–80,000 A/m) were approximately one order larger than saturation magnetization of the ferrofluid (5,252 A/m), thus "demagnetization" field of the non-magnetic particle can still be neglected in the following analysis. Figure 3d shows computed x and y components of the magnetic buoyancy force on a 5 μm particle along line of symmetry ($y' = 0$) of the microchannel. The magnitude of force is on the order of pN. The horizontal component (x) of force changes its polarity at the center of the magnet ($x = 0$). Particles to the left of the magnet experience x-direction deceleration and move slower than the speed of ferrofluids; particles to the right of the magnet experience x-direction acceleration and move faster than the speed of ferrofluids. The vertical y-component of magnetic buoyancy force is always positive. A particle entering the microchannel acquires a non-zero y-direction speed, which leads to its deflection in y-direction as it moves across the channel.

Figure 4a shows simulated trajectories of particles with their diameters ranging from 1 to 10 μm. Flow rate, Q, at the inlet was constant at 5 μl/min. Particles were assumed to enter the microchannel at the center point ($y' = 0$). We found that there was a monotonic increment in the particle deflection (calculated from $|y'(\text{inlet}) - y'(\text{outlet})|$) with increasing particle size. Figure 4b depicts a quadratic relationship between deflections and sizes of particles at

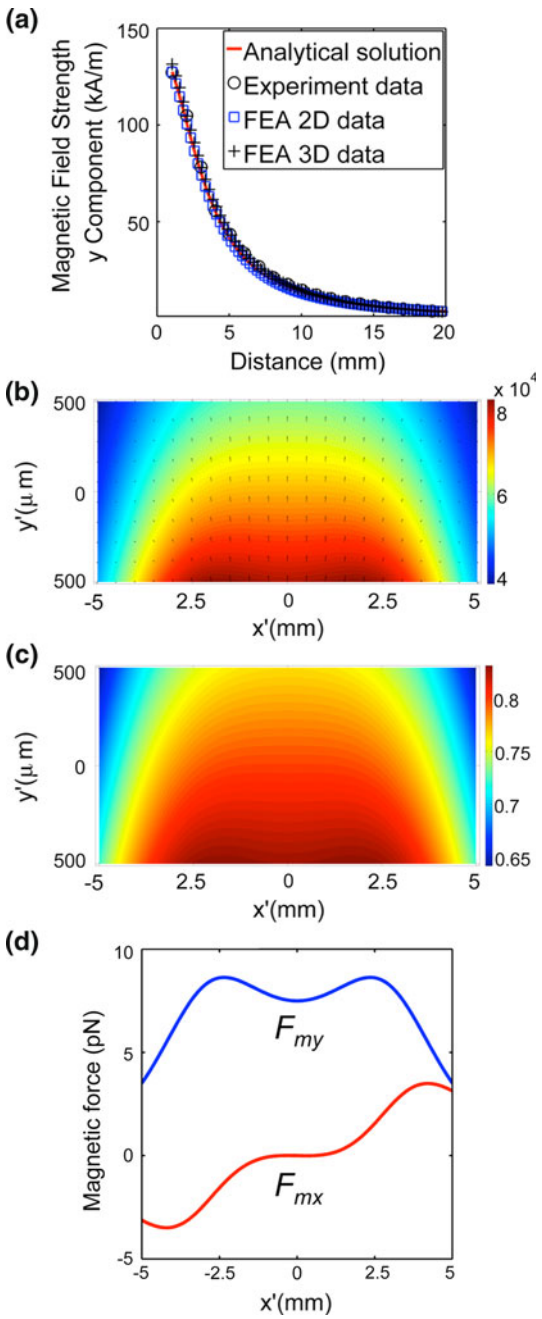

Fig. 3 **a** Comparison of simulated (analytical model and FEA) and measured magnetic field strength produced by the permanent magnet. The magnetization and geometry of the permanent magnet are described in the main text. The plot shows the y-component of the magnetic field strength at the center of the magnet ($z = 0$) decreases as the distance between the surface of the magnet and Hall sensor inside the Gauss meter probe increases. **b** Simulated magnetic field distribution in the microchannel (unit of surface plot: A/m). **c** Simulated normalized ferrofluid magnetization in the microchannel. **d** Simulated x and y components of the magnetic buoyancy force on a 5 μm particle along the line of symmetry ($y' = 0$) in the microchannel

different flow rates. Particles of different diameters were assumed to be flowing at the center-plane in the z-direction of the microchannel, where flow speed of ferrofluids in the

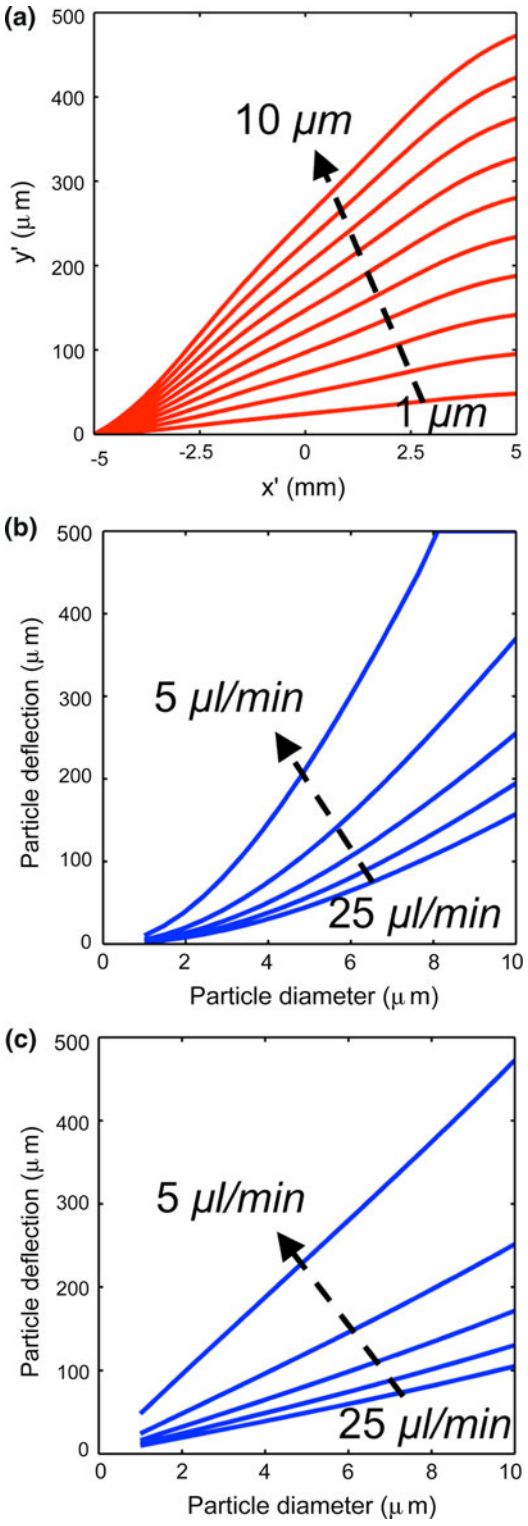

Fig. 4 **a** Simulated trajectories of particles (1 μm to 10 μm in diameter) in the microchannel at a constant flow rate of 5 μl/min. **b** Simulated deflections of particles from the inlet to the outlet (1 cm distance) at different flow rates (5–25 μl/min) when the particles are at the center-plane in the z-direction of the microchannel. **c** Simulated deflections of particles from the inlet to the outlet (1 cm distance) at different flow rates (5–25 μl/min) when the particles are in contact with the channel surface ($z_p = 0$)

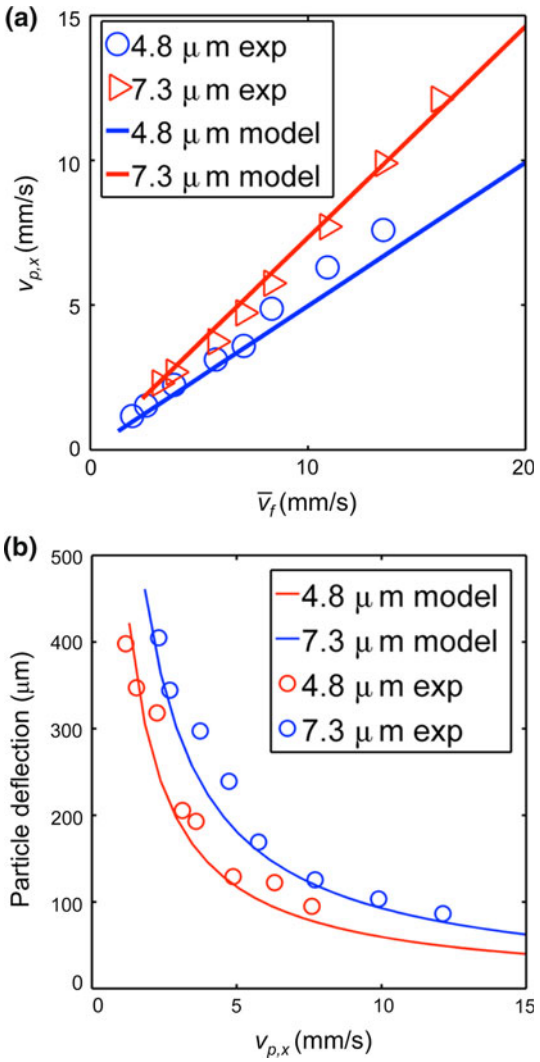

Fig. 5 **a** Simulated and measured speed ($v_{p,x}$) of particles (4.8 μm and 7.3 μm in diameter) when the particles are in contact of the channel surface as a function of the mean flow rate ($\overline{v}_f$) in the microchannel. **b** Simulated and measured deflections of the particles (4.8 μm and 7.3 μm in diameter) when the particles are in contact of the channel surface

x-direction was maximal and constant. Under such condition, the time it takes for particles of different sizes to travel across the microchannel is also constant. The quadratic relationship can then be explained through a simple force analysis. Magnetic buoyancy force is proportional to the volume of the particle (D_p^3), while hydrodynamic viscous drag scales only with the diameter of the particle D_p. Therefore, particle velocity in the y-direction balanced by both magnetic buoyancy and hydrodynamic drag force depends on D_p^2, which explains the quadratic relationship between particle deflections and sizes in theory. In experiments, however, the particles were not flowing at the center-plane in the z-direction of the channel. In fact, virtually all particles were pushed into contact with the

bottom surface of the channel to help the experimenter visualize fluorescence from the particles. Due to the opaqueness of ferrofluids, fluorescent particles are only visible when they are very close to surfaces of the microfluidic channel. In our experiments, to ensure that all particles were close to the bottom surface of the microchannel, we moved the permanent magnet slightly in the positive z-direction. This in turn created a negative z-direction component of magnetic buoyancy force that can push particles towards the bottom surface of the channel. Magnitude of the force is on the order of 1 pN for 2 μm particles, which is much larger than the net force due to gravity and fluid buoyancy of particles. As a result, the particles were quickly pushed towards the bottom surface of the channel, balanced by hydrodynamic viscous drag force, with a mean speed of $\sim$100 μm/s. We observed in the experiments that all particles were pushed onto bottom surface of the channel as soon as they entered the channel. It should be noted that both x and y components of magnetic fields were affected by less than 1% with the permanent magnet being off-centered by 1 mm. In the subsequent simulation, we assumed all particles are at the bottom surface of the channel, which makes $z_p = 0$. In this limit, $f_D = 3$ according to Eq. 18, so that hydrodynamic drag of a particle is three times larger than that when no solid surface was in the vicinity of that particle (Liu et al. 2009; Gijs et al. 2010). Under this condition, the time it takes for particles of different sizes to travel across the microchannel is not constant any more. When a particle is in contact with the surface of the channel, its diameter directly determines the z-location of the particle center and its corresponding flow plane in the z-direction. As a result, larger particles travel faster than smaller ones when $z_p = 0$ in a rectangular microchannel channel. Therefore, larger particles have a shorter residual time in the microchannel compared to small ones, resulting in overall smaller deflections compared to the results obtained in Fig. 4b under the assumption that all particles travel at the same speed. Figure 4c depicts such relationship between deflections and sizes of the particles when $z_p = 0$.

Figure 5a compares measured speeds of the particles (4.8 μm and 7.3 μm in diameters) in experiments extracted from sequential fluorescent images to the simulated particle speeds using the analytical model under $z_p = 0$ condition. These two speeds agreed reasonably well, indicating that particles in the experiments were indeed in contact with the channel surface. Figure 5b shows the comparison between theoretically and experimentally obtained deflections of both 4.8 μm and 7.3 μm particles at different particle velocities. Theoretical deflections were calculated from $|y'(\text{inlet}) - y'(\text{outlet})|$, where $y'(\text{inlet})$ and $y'(\text{outlet})$ were y-locations of particles in the microchannel at the inlet and outlet, respectively. Experimental deflections were extracted from the sequential fluorescent images. Both values again agreed reasonably well, confirming the validity of our analytical model in predicating the trajectories of the particles.

5 Conclusion

We developed an analytical model of transport of non-magnetic spherical microparticles in ferrofluids in a microfluidic system that consists of a microchannel and a permanent magnet. The permanent magnet produced a spatially non-uniform magnetic field that gave rise to a magnetic buoyancy force on particles within the ferrofluid-filled microchannel. We derived the equations of motions for particles using analytical expressions for dominant magnetic buoyancy and hydrodynamic viscous drag forces. The results from the model indicated that the particles would be increasingly deflected in the direction that was perpendicular to the flow when the size of the particles increased, or when the flow rate in the microchannel decreased. "Wall effect" has shown significant consequence on the trajectories and overall deflections of particles. Experimental results confirmed the validity of our analytical model. The analytical model developed in this paper is simple, easy to implement, and useful for quick optimization of future separation and manipulation devices that are based on ferrofluids.

Acknowledgments This research was financially supported by the Office of the Vice President for Research at the University of Georgia, and by the B3I Seed Grant Program with funds from the University of Georgia Research Foundation, Inc.

References

Berkovsky BM, Medvedev VF, Krakov MS (1993) Magnetic fluids: engineering applications. Oxford University Press, New York

Bonner WA, Hulett HR, Sweet RG, Herzenberg LA (1972) Fluorescence activated cell sorting. Rev Sci Instrum 43(3):404–409

Brody JP, Yager P, Goldstein RE, Austin RH (1996) Biotechnology at low Reynolds numbers. Biophys J 71(6):3430–3441

Cho YK, Lee JG, Park JM, Lee BS, Lee Y, Ko C (2007) One-step pathogen specific DNA extraction from whole blood on a centrifugal microfluidic device. Lab Chip 7(5):565–573

Davis JA, Inglis DW, Morton KJ, Lawrence DA, Huang LR, Chou SY, Sturm JC, Austin RH (2006) Deterministic hydrodynamics: taking blood apart. Proc Natl Acad Sci USA 103(40): 14779–14784

Deen WM (1998) Analysis of transport phenomena. Oxford University Press, New York

Di Carlo D (2009) Inertial microfluidics. Lab Chip 9(21):3038–3046

Easley CJ, Karlinsey JM, Bienvenue JM, Legendre LA, Roper MG, Feldman SH, Hughes MA, Hewlett EL, Merkel TJ, Ferrance JP, Landers JP (2006) A fully integrated microfluidic genetic analysis system with sample-in-answer-out capability. Proc Natl Acad Sci USA 103(51):19272–19277

Einstein A (1956) Investigations on the theory of Brownian movement. Dover, New York
Furlani EP (2006) Analysis of particle transport in a magnetophoretic microsystem. J Appl Phys 99(2):024912
Furlani EP, Sahoo Y (2006) Analytical model for the magnetic field and force in a magnetophoretic microsystem. J Phys D 39(9):1724–1732
Ganatos P, Pfeffer R, Weinbaum S (1980) A strong interaction theory for the creeping motion of a sphere between plane parallel boundaries.2. Parallel motion. J Fluid Mech 99:755–783
Gassner AL, Abonnenc M, Chen HX, Morandini J, Josserand J, Rossier JS, Busnel JM, Girault HH (2009) Magnetic forces produced by rectangular permanent magnets in static microsystems. Lab Chip 9:2356–2363
Gijs MAM, Lacharme F, Lehmann U (2010) Microfluidic applications of magnetic particles for biological analysis and catalysis. Chem Rev 110(3):1518–1563
Gossett DR, Weaver WM, Mach AJ, Hur SC, Tse HTK, Lee W, Amini H, Di Carlo D (2010) Label-free cell separation and sorting in microfluidic systems. Anal Bioanal Chem 397(8): 3249–3267
Han KH, Frazier AB (2004) Continuous magnetophoretic separation of blood cells in microdevice format. J Appl Phys 96(10): 5797–5802
Huang LR, Cox EC, Austin RH, Sturm JC (2004) Continuous particle separation through deterministic lateral displacement. Science 304(5673):987–990
Ichikawa N, Hosokawa K, Maeda R (2004) Interface motion of capillary-driven flow in rectangular microchannel. J Colloid Interface Sci 280(1):155–164
Jones TB (1995) Electromechanics of particles. Cambridge University Press, Cambridge
Kose AR, Fischer B, Mao L, Koser H (2009) Label-free cellular manipulation and sorting via biocompatible ferrofluids. Proc Natl Acad Sci USA 106(51):21478–21483
Krebs MD, Erb RM, Yellen BB, Samanta B, Bajaj A, Rotello VM, Alsberg E (2009) Formation of ordered cellular structures in suspension via label-free negative magnetophoresis. Nano Lett 9(5):1812–1817
Krishnan GP, Leighton DT (1995) Inertial lift on a moving sphere in contact with a plane wall in a shear-flow. Phys Fluids 7(11): 2538–2545
Kumar A, Bhardwaj A (2008) Methods in cell separation for biomedical application: cryogels as a new tool. Biomed Mater 3(3):034008
Laurell T, Petersson F, Nilsson A (2007) Chip integrated strategies for acoustic separation and manipulation of cells and particles. Chem Soc Rev 36(3):492–506
Lee H, Purdon AM, Chu V, Westervelt RM (2004) Controlled assembly of magnetic nanoparticles from magnetotactic bacteria using microelectromagnets arrays. Nano Lett 4(5):995–998
Leighton D, Acrivos A (1985) The lift on a small sphere touching a plane in the presence of a simple shear flow. Z Angew Math Phys 36:174–178
Li J, Zhang Z, Rosenzweig J, Wang YY, Chan DW (2002) Proteomics and bioinformatics approaches for identification of serum biomarkers to detect breast cancer. Clin Chem 48(8): 1296–1304
Liu C, Stakenborg T, Peeters S, Lagae L (2009) Cell manipulation with magnetic particles toward microfluidic cytometry. J Appl Phys 105(10):102011–102014
Mao L, Koser H (2005) Ferrohydrodynamic pumping in spatially traveling sinusoidally time-varying magnetic fields. J Magn Magn Mater 289:199–202
Mao LD, Koser H (2006) Towards ferrofluidics for mu-TAS and lab on-a-chip applications. Nanotechnology 17(4):S34–S47
Miltenyi S, Muller W, Weichel W, Radbruch A (1990) High gradient magnetic cell separation with MACS. Cytometry 11(2):231–238
Mirica KA, Shevkoplyas SS, Phillips ST, Gupta M, Whitesides GM (2009) Measuring densities of solids and liquids using magnetic levitation: fundamentals. J Am Chem Soc 131(29):10049–10058
Mirica KA, Phillips ST, Mace CR, Whitesides GM (2010) Magnetic levitation in the analysis of foods and water. J Agric Food Chem 58(11):6565–6569
Muldoon LL, Sandor M, Pinkston KE, Neuwelt EA (2005) Imaging, distribution, and toxicity of superparamagnetic iron oxide magnetic resonance nanoparticles in the rat brain and intracerebral tumor. Neurosurgery 57(4):785–796
Nagrath S, Sequist LV, Maheswaran S, Bell DW, Irimia D, Ulkus L, Smith MR, Kwak EL, Digumarthy S, Muzikansky A, Ryan P, Balis UJ, Tompkins RG, Haber DA, Toner M (2007) Isolation of rare circulating tumour cells in cancer patients by microchip technology. Nature 450(7173):1235–1239
Odenbach S (2002) Ferrofluids: magnetically controllable fluids and their applications. Springer, London
Pamme N (2006) Magnetism and microfluidics. Lab Chip 6(1):24–38
Pamme N (2007) Continuous flow separations in microfluidic devices. Lab Chip 7(12):1644–1659
Pamme N, Manz A (2004) On-chip free-flow magnetophoresis: continuous flow separation of magnetic particles and agglomerates. Anal Chem 76(24):7250–7256
Pamme N, Wilhelm C (2006) Continuous sorting of magnetic cells via on-chip free-flow magnetophoresis. Lab Chip 6(8):974–980
Pankhurst QA, Connolly J, Jones SK, Dobson J (2003) Applications of magnetic nanoparticles in biomedicine. J Phys D 36(13): R167–R181
Petersson F, Aberg L, Sward-Nilsson AM, Laurell T (2007) Free flow acoustophoresis: microfluidic-based mode of particle and cell separation. Anal Chem 79(14):5117–5123
Peyman SA, Kwan EY, Margarson O, Iles A, Pamme N (2009) Diamagnetic repulsion—a versatile tool for label-free particle handling in microfluidic devices. J Chromatogr A 1216(52): 9055–9062
Pham P, Masse P, Berthier J (2000) Numerical modeling of superparamagnetic sub-micronic particles trajectories under the coupled action of 3D force fields. Eur Phys J Appl Phys 12(3):211–216
Pieranski P, Clausen S, Helgesen G, Skjeltorp AT (1996) Braids plaited by magnetic holes. Phys Rev Lett 77(8):1620–1623
Rosensweig RE (1966) Fluidmagnetic buoyancy. AIAA J 4:1751–1758
Rosensweig RE (1985) Ferrohydrodynamics. Cambridge University Press, Cambridge
Rosensweig RE, Lee WK, Siegell JH (1987) Magnetically stabilized fluidized-beds for solids separation by density. Sep Sci Technol 22(1):25–45
Schuler D, Frankel RB (1999) Bacterial magnetosomes: microbiology, biomineralization and biotechnological applications. Appl Microbiol Biol 52(4):464–473
Shi JJ, Huang H, Stratton Z, Huang YP, Huang TJ (2009) Continuous particle separation in a microfluidic channel via standing surface acoustic waves (SSAW). Lab Chip 9(23):3354–3359
Skjeltorp AT (1983) One- and two-dimensional crystallization of magnetic holes. Phys Rev Lett 51(25):2306–2309
Smistrup K, Hansen O, Bruus H, Hansen MF (2005) Magnetic separation in microfluidic systems using microfabricated electromagnets—experiments and simulations. J Magn Magn Mater 293:597–604
Toner M, Irimia D (2005) Blood-on-a-chip. Annu Rev Biomed Eng 7:77–103
Tsutsui H, Ho CM (2009) Cell separation by non-inertial force fields in microfluidic systems. Mech Res Commun 36(1):92–103
Voldman J (2006) Electrical forces for microscale cell manipulation. Annu Rev Biomed Eng 8:425–454

Weissleder R, Stark DD, Engelstad BL, Bacon BR, Compton CC, White DL, Jacobs P, Lewis J (1989) Superparamagnetic iron-oxide—pharmacokinetics and toxicity. Am J Roentgenol 152(1): 167–173

Willard MA, Kurihara LK, Carpenter EE, Calvin S, Harris VG (2004) Chemically prepared magnetic nanoparticles. Int Mater Rev 49(3-4):125–170

Winkleman A, Perez-Castillejos R, Gudiksen KL, Phillips ST, Prentiss M, Whitesides GM (2007) Density-based diamagnetic separation: devices for detecting binding events and for collecting unlabeled diamagnetic particles in paramagnetic solutions. Anal Chem 79(17):6542–6550

Wirix-Speetjens R, Fyen W, Xu KD, De Boeck J, Borghs G (2005) A force study of on-chip magnetic particle transport based on tapered conductors. IEEE Trans Magn 41(10):4128–4133

Xia Y, Whitesides GM (1998) Soft lithography. Annu Rev Mater Res 28(1):153–184

Yamada M, Seki M (2005) Hydrodynamic filtration for on-chip particle concentration and classification utilizing microfluidics. Lab Chip 5(11):1233–1239

Yamada M, Nakashima M, Seki M (2004) Pinched flow fractionation: continuous size separation of particles utilizing a laminar flow profile in a pinched microchannel. Anal Chem 76(18):5465–5471

Yellen BB, Hovorka O, Friedman G (2005) Arranging matter by magnetic nanoparticle assemblers. Proc Natl Acad Sci USA 102(25):8860–8864

Yung CW, Fiering J, Mueller AJ, Ingber DE (2009) Micromagnetic-microfluidic blood cleansing device. Lab Chip 9(9):1171–1177

Zborowski M, Ostera GR, Moore LR, Milliron S, Chalmers JJ, Schechter AN (2003) Red blood cell magnetophoresis. Biophys J 84(4):2638–2645

Zhu TT, Marrero F, Mao LD (2010) Continuous separation of non-magnetic particles inside ferrofluids. Microfluid Nanofluid 9(4–5):1003–1009